

## Article

# Recycling of Valuable Metals from the Priority Lithium Extraction Residue Obtained through Hydrogen Reduction of Spent Lithium Batteries

Yong Guo, Fupeng Liu \*, Feixiong Chen, Zaoming Chen \*, Hong Zeng, Tao Zhang and Changquan Shen

Yichun Lithium New Energy Industry Research Institute, Jiangxi University of Science and Technology, Ganzhou 341000, China; 18679758281@163.com (Y.G.); 15579880267@139.com (F.C.); 18370477088@163.com (C.S.)

\* Correspondence: fupengliu@126.com (F.L.); chenzaoming@126.com (Z.C.); Tel.: +86-188-7979-6708 (F.L.); Fax: +86-0797-8312-422 (F.L.)

**Abstract:** The selective separation of lithium from spent ternary positive materials is achieved through hydrogen reduction followed by water leaching. Almost 98% of the Li is transformed into soluble  $\text{LiOH}\cdot\text{H}_2\text{O}$ , while the Ni, Co and Mn species are all transformed into insoluble metals or their oxides, so the recovery of Ni, Co and Mn at this stage is challenging. The traditional acid leaching process has drawbacks such as high oxidant consumption, the low recovery of valuable metals and high production costs. Thus, sulfation roasting followed by water leaching was studied in this project. The leaching levels of Ni, Co, Mn and Al reached 87.13%, 99.87%, 96.21% and 94.95%, respectively, with 1.4 times the theoretical amount of sulfuric acid used at 180 °C for 120 min. To avoid the adverse effects of Mn and Al on the quality of the Ni and Co sulfate products,  $\text{Mn}^{2+}$  was first separated and precipitated via the  $\text{KMnO}_4$  oxidation–precipitation method, and >98% of the Mn was removed and precipitated within 30 min with a  $K_p/K_t$  (ratio of actual usage to theoretical usage of  $\text{KMnO}_4$ ) of 1.0 at pH = 2.0 and 25 °C. After removal of the Mn, the solvent extraction method was adopted by using P204 as an extractant to separate Al. More than 98% of the Al was extracted in 30 min with 20% (v/v) P204 + 10% (v/v) TBP with an A/O ratio of 1:1 at 30 °C. This optimized process for extracting lithium residues improved the hydrogen reduction process of waste lithium batteries and will enable industrialization of the developed processes.

**Keywords:** spent lithium batteries; hydrogen reduction; sulfation roasting; lithium; aluminum removal



**Citation:** Guo, Y.; Liu, F.; Chen, F.; Chen, Z.; Zeng, H.; Zhang, T.; Shen, C. Recycling of Valuable Metals from the Priority Lithium Extraction Residue Obtained through Hydrogen Reduction of Spent Lithium Batteries. *Batteries* **2024**, *10*, 28. <https://doi.org/10.3390/batteries10010028>

Academic Editors: Leiting Shen, Yongming Chen, Changhong Wang and Jae-won Lee

Received: 2 December 2023

Revised: 26 December 2023

Accepted: 8 January 2024

Published: 11 January 2024



**Copyright:** © 2024 by the authors. Licensee MDPI, Basel, Switzerland. This article is an open access article distributed under the terms and conditions of the Creative Commons Attribution (CC BY) license (<https://creativecommons.org/licenses/by/4.0/>).

## 1. Introduction

Lithium batteries are characterized by high energy ratios, high voltages, efficient reversibility, safety and stability. Lithium batteries are rapidly becoming indispensable power sources for smart devices, electric vehicles and other products due to their excellent performance [1,2]. However, on average, the maximum charge and discharge cycles of lithium batteries are 1000 [3,4]. This means that many lithium batteries will become obsolete as they reach the end of their useful life. It is expected that the end-of-life powers of the lithium batteries in China will reach 134.5 Gwh by 2025 [5–7]. As spent lithium batteries contain large amounts of heavy metals and toxic electrolytes, this could potentially bring great harm to the environment [8]. Therefore, the recovery of valuable metals from spent lithium-ion batteries has attracted significant attention in academia and industry [9].

At present, the main methods for treating waste lithium batteries include the pyrometallurgical method [10], hydrometallurgical method [11,12], and the combined process of pyrometallurgy and hydrometallurgy. However, there are many shortcomings in the pyrometallurgical process used in treating spent lithium batteries, such as low lithium recovery rates, high energy consumption [13] and secondary pollution from waste gases and residues [14]. Therefore, the utilization of waste lithium batteries in China is mainly

based on hydrometallurgical processes [15]. The conventional hydrometallurgical process includes sulfuric acid reduction leaching; iron precipitation; nickel, cobalt and manganese extraction and separation; and lithium salt concentration and precipitation [16]. Although the operations of this process are relatively simple, the processing time is long. It is particularly difficult to accomplish selective leaching of lithium, and lithium is lost in each process. The total yield of lithium is only 60–80% [17].

Considering the drawbacks of single hydrometallurgical or pyrometallurgical processes in recycling lithium-ion batteries, combined pyro-hydrometallurgical processes have gained increasing attention in industry, such as carbon reduction roasting–low-acid leaching, sulfation roasting–water leaching, and nitration roasting–water leaching. The “sulfation roasting–water leaching”, “nitrification roasting–water leaching” and “carbon reduction roasting–low-acid leaching” processes selectively convert most of the Li (90%) into water-soluble nitrate, sulfate or carbonate salts through reduction roasting, while the other elements remain as insoluble oxides or metals [18–21]. The selective extraction of Li can be achieved through water leaching. However, the roasting process used in the treatment of spent lithium batteries generates NO, CO, CO<sub>2</sub>, NO<sub>2</sub>, SO<sub>2</sub> and other pollutants. In addition, the roasting kinetics are relatively slow, and the lithium in the cathode can only be completely converted into nitrate, sulfate or carbonate salt when the roasting time is more than 2 h [22,23]. Therefore, in response to the many deficiencies of the combined method described above, a green and environmentally friendly hydrogen reduction process was developed by our research group [24]. This technology first utilized hydrogen reduction to convert the Li in spent lithium batteries into LiOH, which is very soluble in water, and then, selectively extracted the lithium via water leaching. Previous exploratory experiments showed that almost 98% of the Li in spent lithium batteries was selectively transformed within 15 min at 500 °C when the hydrogen reduction process was used [25]. More importantly, the temperature of hydrogen reduction roasting is significantly lower than carbon reduction roasting (650 °C) and sulfate roasting (975 °C), and the energy consumption is significantly reduced. The advantage of this technology is that no harmful gases are generated during the reduction roasting process, and lithium separation can be achieved without consuming any acid or alkali [26]. Another advantage of this technology is that battery-grade LiOH·H<sub>2</sub>O can be obtained without complicated separation and purification steps. Overall, hydrogen reduction roasting for transformational recovery is a simple, efficient and environmentally friendly method with great potential for industrial application [27].

When adopting hydrogen a reduction roasting process, lithium is selectively extracted and separated through water leaching. However, Ni, Co and Mn compounds are all converted to the corresponding insoluble metals or their oxides. It is difficult to recover the roasting reduction products, and Ni, Co and Mn are important raw materials for the production of lithium batteries. Therefore, the recovery of Ni, Co and Mn from priority lithium extraction residue is challenging and important. The traditional treatment uses sulfuric acid leaching and hydrogen peroxide as the oxidant, but the leaching efficiency of Li is low, and a large amount of oxidant is introduced. To ensure the integrity of hydrogen reduction in processing spent lithium batteries, a sulfation roasting–water leaching process was developed for the recovery of Ni, Co and Mn from priority lithium extraction residues. To prepare high-purity nickel sulfate and cobalt sulfate, Mn<sup>2+</sup> was selectively precipitated by potassium permanganate (KMnO<sub>4</sub>) as MnO<sub>2</sub> or Mn<sub>2</sub>O<sub>3</sub>, and a solvent extraction process was used with P2O4 (di(2-ethylhexyl) phosphate) as the extractant to achieve selective separation of Al.

## 2. Experimental Section

### 2.1. Materials and Characterization

The spent ternary battery material was pretreated (disassembled, sieved, milled), and then, most of the Li was transformed into soluble  $\text{LiOH}\cdot\text{H}_2\text{O}$  through hydrogen reduction roasting. Almost all of the Li in the roasted material was separated from other impurities through water leaching. The raw material for these experiments came from a priority lithium extraction residue after hydrogen reduction roasting. Ni, Co and Mn compounds were converted to the corresponding metals or oxides. They were then subjected to chemical composition analyses, an XRD phase analysis and a SEM–EDS analysis. The chemical composition of the priority lithium extraction residue is presented in Table 1, and the main metals present were Ni, Co and Mn. The contents of Ni, Co, Mn and Al were 11.00%, 17.44%, 4.40% and 4.48%, respectively. Characterization of the LIB waste by XRD is shown in Figure 1, which revealed that Ni and Co were mainly present as metals, and Mn and Al were present as  $\text{MnO}$  and  $\text{Al}_2\text{O}_3$ , respectively. Characterization of the LIB waste with an elemental distribution map, as shown in Figure 2, revealed that the Ni and Co distribution areas overlapped each other, and the Al, Cu and Ca elements were all dispersed. The average particle size of the priority lithium extraction residue was  $41.6\ \mu\text{m}$ . Figure 3 and Table 2 present the SEM–EDS results for different spots, which confirm the presence of Ni, Co and  $\text{MnO}$  as well as the main phases in the priority lithium extraction residue.

**Table 1.** Chemical components of the priority lithium extraction residue.

Elements	Ni	Co	Mn	Al	Cu	Fe
wt.%	11.00	17.44	4.40	4.88	11.29	0.58

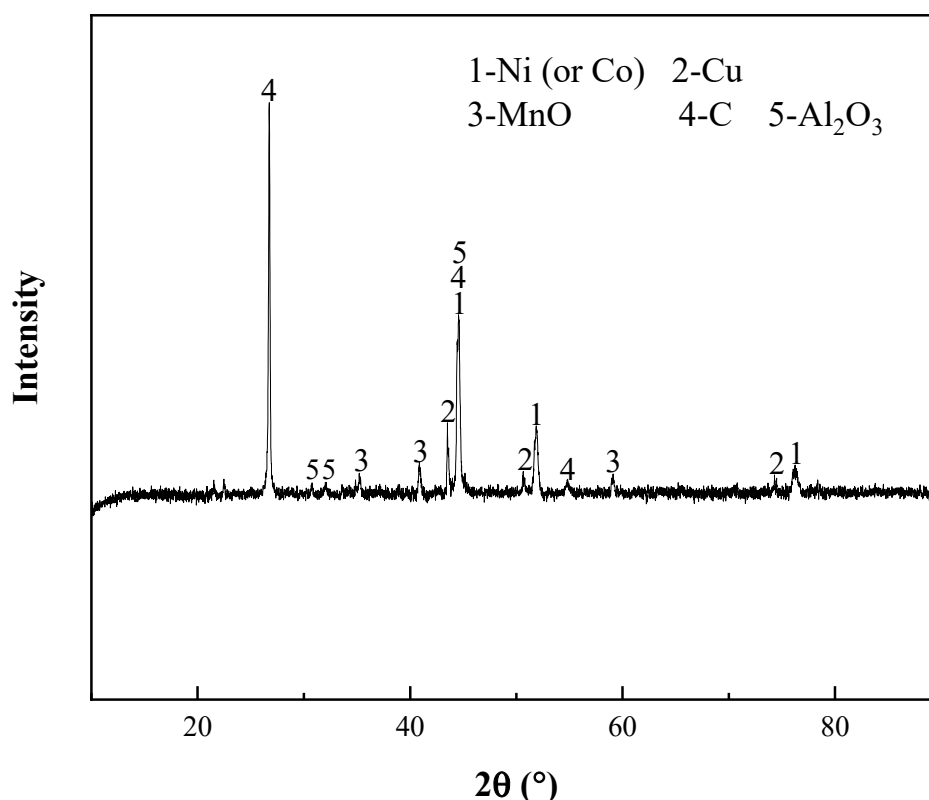


**Figure 1.** XRD data for the priority lithium extraction residue.

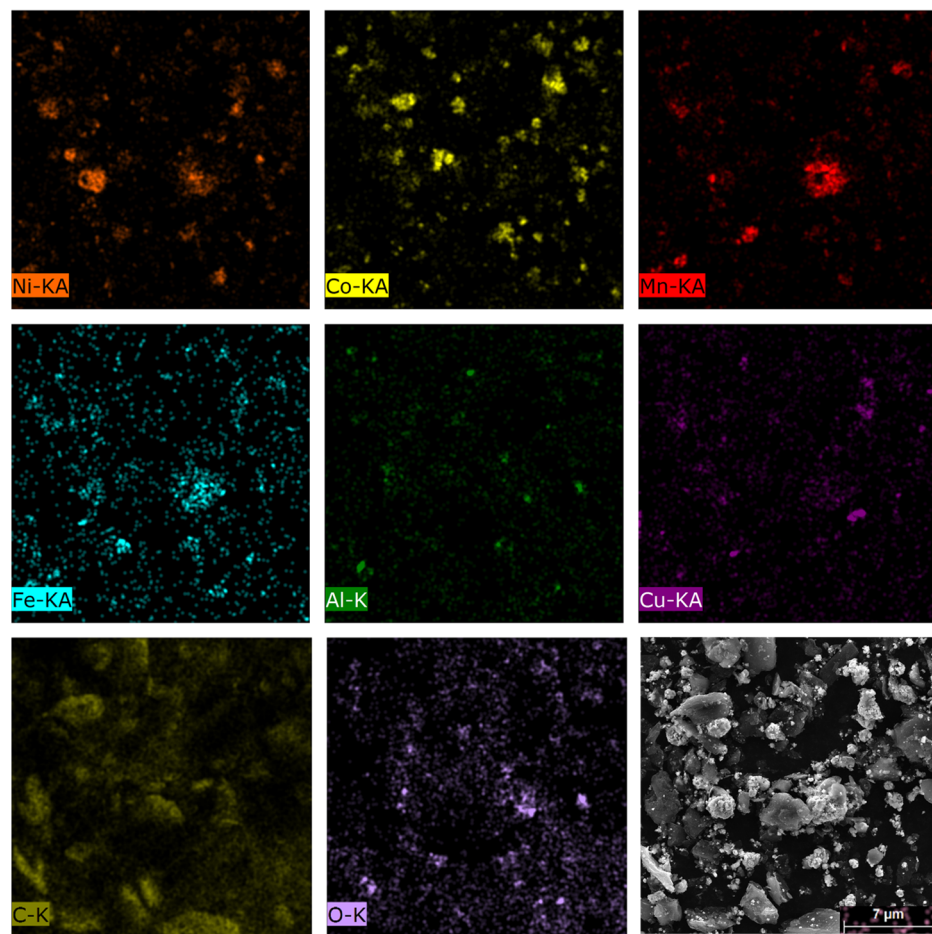


**Figure 2.** Distribution maps for the main elements present in the priority lithium extraction residue.

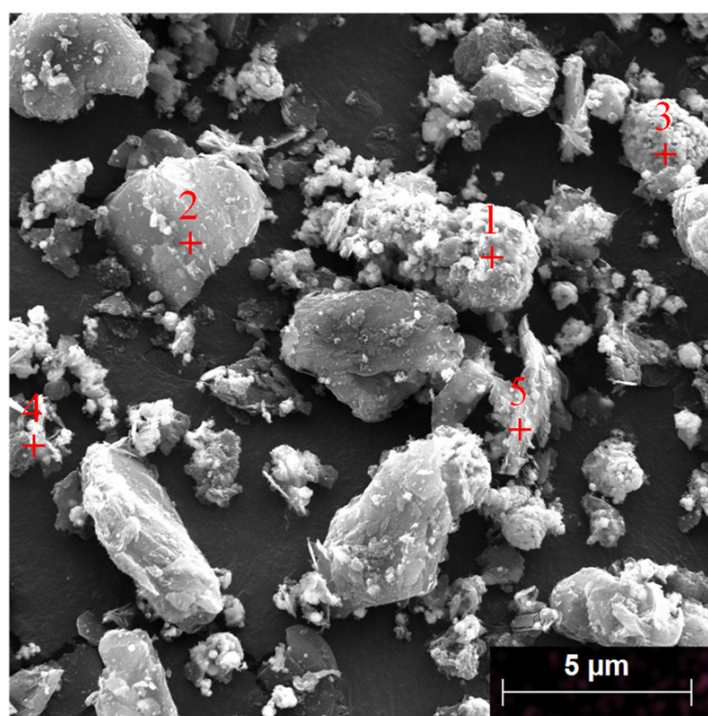


**Figure 3.** SEM-EDS image of the priority lithium extraction residue.

**Table 2.** SEM-EDS analysis results of the spots shown in Figure 3.

Spectrum	O	Mn	Co	Ni	Al	Fe	Cu
1	50.66	45.91	1.47	0.27	0.20	0.38	1.24
2	7.68	3.47	84.74	1.34	0.32	0.15	2.30
3	7.37	4.07	4.26	81.28	0.27	0.14	2.61
4	7.77	2.00	84.01	1.76	0.00	0.00	4.47
5	36.45	7.95	30.10	16.71	2.33	0.00	6.45

## 2.2. Experimental Procedures

Priority lithium residues came from the hydrogen reduction roasting–water leaching process. The conditions of the hydrogen reduction roasting process were  $T = 500\text{ }^{\circ}\text{C}$ ,  $t = 15\text{ min}$  and a hydrogen flow rate of  $200\text{ mL/min}$ . After hydrogen reduction roasting, water leaching was performed with a liquid-to-solid ratio of  $20:1$  for  $30\text{ min}$  at a temperature of  $30\text{ }^{\circ}\text{C}$  [24]. After liquid–solid separation, the priority leaching residue was obtained.

Sulfation roasting process: the solid was weighed in a crucible with an electronic balance (JA1003N, Shanghai Jingketianmei Scientific Instrument Co., Ltd., Shanghai, China), and the Ni, Co, Mn and Al contents were determined after a complete reaction with sulfuric acid ( $18.4\text{ mol/L}$ ) to produce the corresponding sulphates. Concentrated sulfuric acid was added and mixed quickly for powder maturation. After maturation, the crucible was weighed, and then, placed in a muffle furnace (KSL-1200X, Hefei Kejing Material Technology Co., Ltd., Hefei, China.). The temperature controller was programmed for a  $5\text{--}6\text{ }^{\circ}\text{C}/\text{min}$  rise. When the temperature rose to the predetermined temperature, it was held there, the reaction began, and then, the crucible was cooled when the reaction was over. When the temperature dropped to room temperature, the crucible was weighed again after roasting. Thus, the increase in the mass of the material was calculated after roasting, and the content of each element in the roasted product was calculated. The elemental contents of the roasted product were calculated with Equation (1).

The conditions for the water leaching experiment were a L/S (liquid-to-solid ratio) of  $10:1\text{ mL/g}$ , a leaching time of  $120\text{ min}$  and a leaching temperature of  $25\text{ }^{\circ}\text{C}$ . The experiments were carried out in a thermostatted water bath shaker (SHZ-88, Shanghai Jinghai Instrument Co., Ltd., Shanghai, China) with an oscillation frequency of  $250\text{ rpm}$  and an oscillation amplitude of  $20\text{ mm}$ . The analyses and calculations included determinations of the leaching rates with ICP (Perkin Elmer Optima 7100 DV, Waltham, MA, USA) measurements of the metal concentrations in the leachate and the transformations and XRD (PANalytical X'Pert Pro Powder, Almelo, The Netherlands) and SEM-EDS (MIRA 3 LMH, TESCAN Brno, S.r.o., Brno, Czech Republic) analyses of the morphological changes occurring during sulfation roasting. The ionic leaching rates were calculated with Equation (2), and ion leaching refers to the ion content of the leachate as a percentage of the ion content of the roast product.

$$w = \frac{m_0 \times w_0}{m_1} \times 100\% \quad (1)$$

$$E = \frac{C \times V}{m \times w} \times 100\% \quad (2)$$

where  $m_0$  (g) and  $m_1$  (g) are the mass of the material before and after roasting, respectively,  $w_0$  (%) is the content of the element in the material before roasting,  $C$  (g/L) represents the concentrations of the metal ions in the leaching solution,  $V$  (L) is the volume of the leaching solution and  $m$  (g) is the mass of the roasted product.

To selectively separate Mn, a  $\text{KMnO}_4$  solid was added to the leaching solution in a  $100\text{ mL}$  glass beaker equipped with a magnetic stirrer at  $25\text{ }^{\circ}\text{C}$  for  $30\text{ min}$ . Ni, Co, Mn and Al precipitation was investigated with different amounts of  $\text{KMnO}_4$  and pH. The concentration of each metal ion in the leaching solution was measured via ICP, and the precipitation yield was calculated.

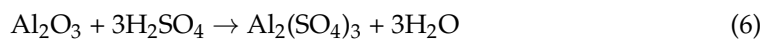
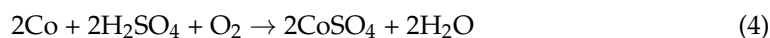
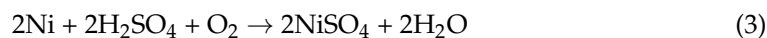
The solvent extraction experiments were carried out by mechanically shaking the organic and aqueous phases in separating funnels. The shaking speed and temperature were set and controlled with a digital water bath oscillator (Shanghai Lichen Instrument Technology Co., Ltd., Shanghai, China). The metal extraction experiments were performed with separatory funnels (125 mL) by mixing the organic phase and the aqueous solution for 30 min at 25 °C. The Al, Ni and Co extractions were investigated with P2O4 as the extractant with different organic/aqueous phase (O/A) ratios and saponification amounts. The concentration of each metal ion in the extract solution was measured via ICP, and the extraction rate was calculated.

### 3. Results and Discussion

#### 3.1. Sulfation Roasting

##### 3.1.1. Experimental Principles

This study used the “sulfation roasting–water leaching” process and converted the valuable metals in the priority lithium extraction product to the corresponding sulphates by roasting with sulfuric acid. The sulphates were leached into solution via water leaching. The main reactions that occurred during the process are shown in Equations (3)–(6).



All thermodynamic data used for the plots were obtained from HSC Chemical 6.0 software. The reactions were those outlined in Equations (3)–(6), and the Gibbs free energies as a function of temperature were plotted for these reactions, as shown in Figure 4. The thermodynamic calculations showed that Co reacted more readily with sulfuric acid than the other metals to form soluble sulphates, which led to higher extraction efficiency for Co relative to the other metals.

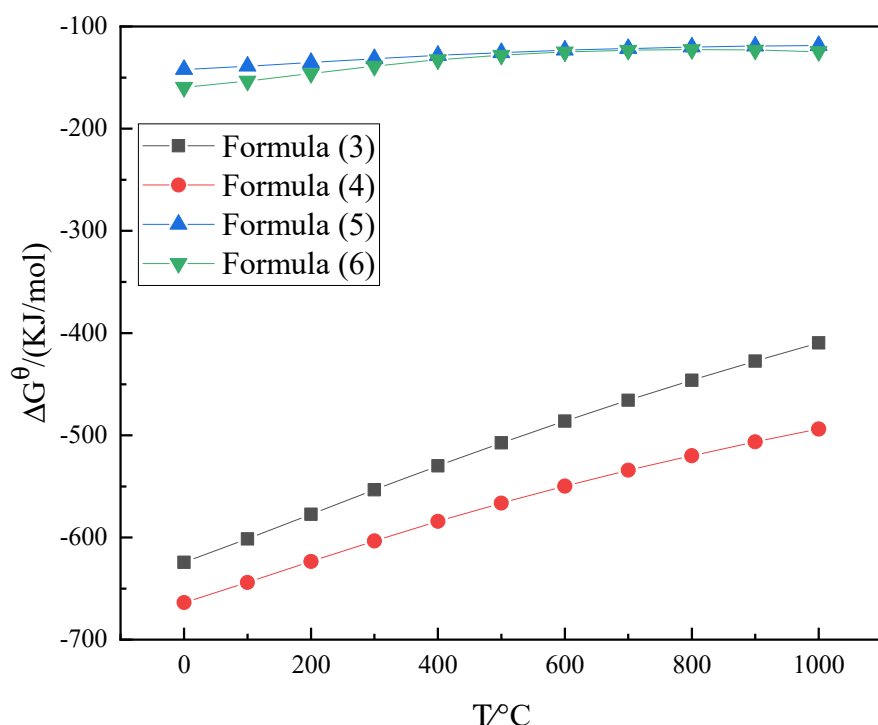


**Figure 4.** Plot of the Gibbs free energies for Equations (3)–(6) versus temperature.

The predominant region diagrams for the Me (Ni, Co and Mn)-S-O system at 200 °C and 250 °C are shown in Figure 5 and were drawn using FactSage8.1 [28]. The results showed that Ni, Co and Mn could be transformed into the corresponding sulphates with high oxidation and sulfidation potentials. Conversely, with low oxidation potentials, these metals would be converted into their corresponding oxides or sulfides. In addition, the temperature had a significant impact on the distribution area of the sulphates. As the roasting temperature increased, the predominant region for the sulfates obviously diminished. This made it difficult to separate and recycle Ni, Co and Mn. Therefore, the sulfation roasting process should be carried out at the right temperatures.

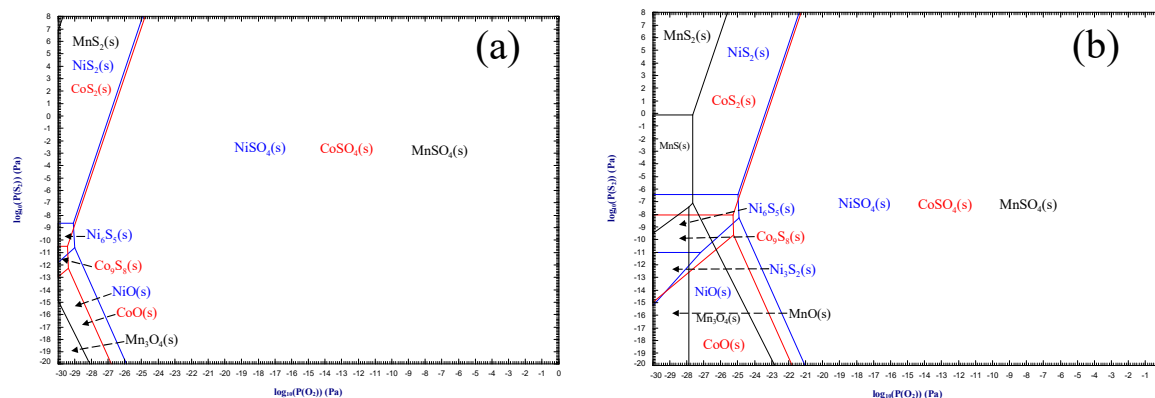


**Figure 5.** Diagrams showing the predominant regions for the Me (Ni, Co and Mn)-S-O system at (a) 200 °C and (b) 250 °C.

### 3.1.2. Effect of the Roasting Temperature

The effects of the roasting temperature on the extractions of Ni, Co, Mn and Al are presented in Figure 6. These results suggest that the roasting temperature had a significant effect on the transformations of Ni, Co, Mn and Al. The yield from Ni extraction increased from 60.02% to 73.45% when the temperature was increased from 140 °C to 180 °C, while the conversion rates for Co, Mn and Al reached 92.95%, 89.76% and 93.62%, respectively. This is clearly illustrated in Figure 7, which shows that the main phases of the roasting products were sulphates, but the nickel metal phase still caused a decrease in the Ni extraction efficiency. When the roasting temperature was increased to 220 °C, the diffraction peaks for  $\text{NiSO}_4 \cdot \text{H}_2\text{O}$ ,  $\text{CoSO}_4 \cdot \text{H}_2\text{O}$ ,  $\text{MnSO}_4 \cdot \text{H}_2\text{O}$  and  $\text{Al}_2(\text{SO}_4)_3 \cdot x\text{H}_2\text{O}$  were still present, diffraction peaks for  $\text{Al}_2(\text{SO}_4)_3$  were also observed, and the diffraction peak for  $\text{Al}_2(\text{SO}_4)_3 \cdot x\text{H}_2\text{O}$  gradually decreased. This indicated that at this temperature, some of the  $\text{Al}(\text{HSO}_4)_3$  decomposed to form  $\text{Al}_2(\text{SO}_4)_3 \cdot x\text{H}_2\text{O}$ , and  $\text{Al}_2(\text{SO}_4)_3 \cdot x\text{H}_2\text{O}$  lost its waters of crystallization and was converted to anhydrous  $\text{Al}_2(\text{SO}_4)_3$ . Figure 8 shows that C, Ni and  $\text{Al}_2\text{O}_3$  were the main mineral phases formed at 140 °C after water leaching, which indicated that the metal extraction yields were low because the reaction temperature was not high enough. A further increase in the roasting temperature to 180–220 °C resulted in only minor changes in the Ni, Co, Mn and Al extraction yields.

### 3.1.3. Effect of Roasting Time

The effect of roasting time on the extraction of Ni, Co, Mn and Al is presented in Figure 9. Roasting time had little effect on metal leaching. The leaching of Ni, Co, Mn and Al stabilized after a slow rise. When the roasting time was increased from 30 min to 60 min, the Ni extraction efficiency increased from 63.69 to 69.75%; conversely, the extraction efficiencies of Co, Mn and Al increased slowly—Co: 89.60% to 93.30%; Mn: 87.28% to 90.01%; and Al: 80% to 86.28%, respectively. Further increases in roasting time beyond 60 min only resulted in slight increases in the levels of Ni, Co, Mn and Al extraction. This is clearly illustrated in Figure 10, which shows that the main phases within the calcine after 30 min were Ni,  $\text{NiSO}_4 \cdot \text{H}_2\text{O}$ ,  $\text{CoSO}_4 \cdot \text{H}_2\text{O}$ ,  $\text{MnSO}_4 \cdot \text{H}_2\text{O}$ ,  $\text{Al}(\text{HSO}_4)_3$  and

$\text{Al}_2(\text{SO}_4)_3 \cdot x\text{H}_2\text{O}$ . When the roasting time was increased to 150 min, the diffraction peaks for  $\text{Al}(\text{HSO}_4)_3$  disappeared, and diffraction peaks for  $\text{Al}_2(\text{SO}_4)_3$  appeared. This showed that as the roasting time was increased,  $\text{Al}(\text{HSO}_4)_3$  decomposed to form  $\text{Al}_2(\text{SO}_4)_3$ . Figure 11 shows that C and Ni were the main mineral phases following water leaching. This explains the low extraction efficiency for Ni.

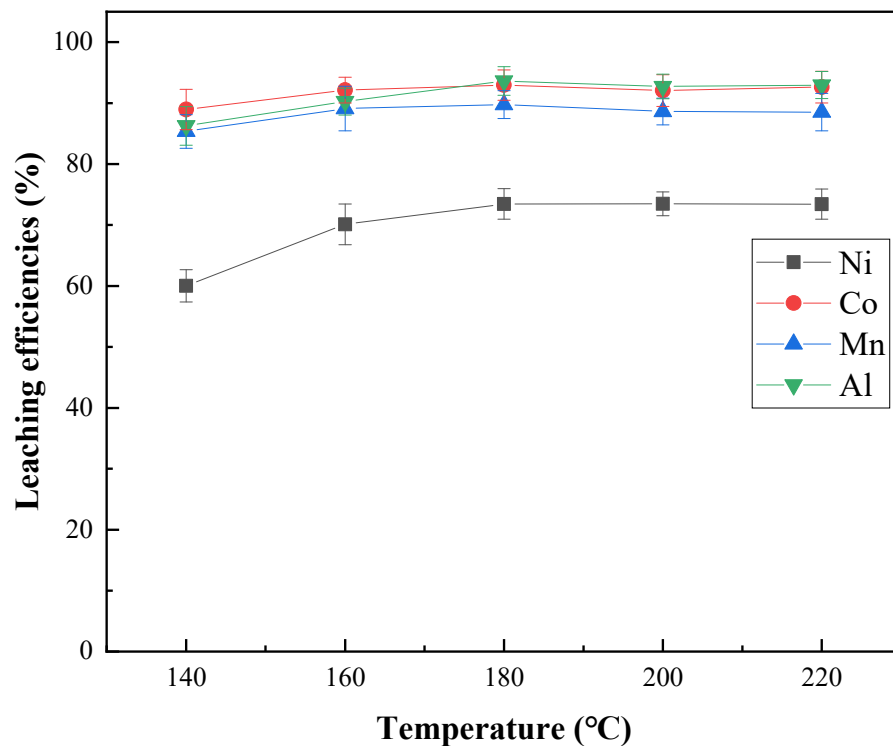


**Figure 6.** Effect of roasting temperature on the leaching efficiency for each element ( $D_p/D_t = 1.2$ ,  $t = 120$  min).

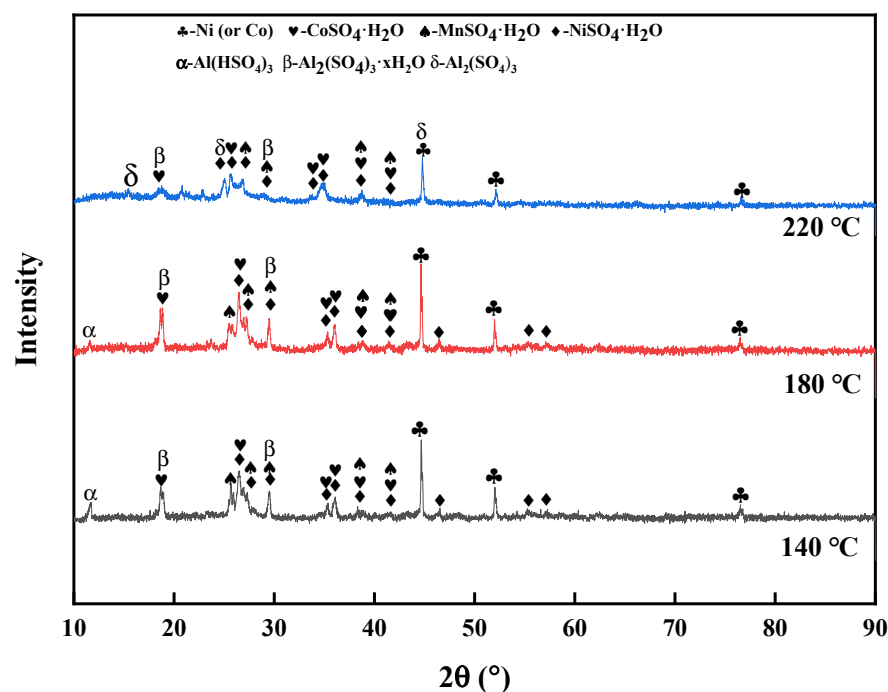


**Figure 7.** X-ray diffraction patterns for the roasting products formed at different roasting temperatures in the sulfate roasting ( $D_p/D_t = 1.2$ ,  $t = 120$  min).

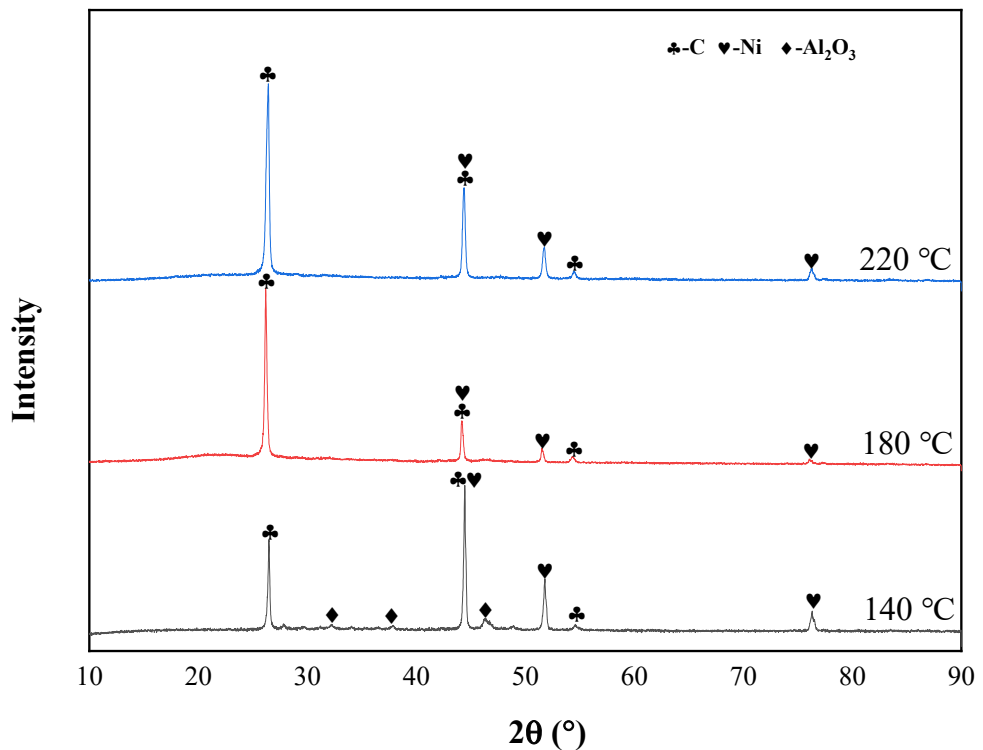


**Figure 8.** X-ray diffraction patterns for the water leaching residues formed at different roasting temperatures ( $t = 120$  min, L/S = 10 mL/g).

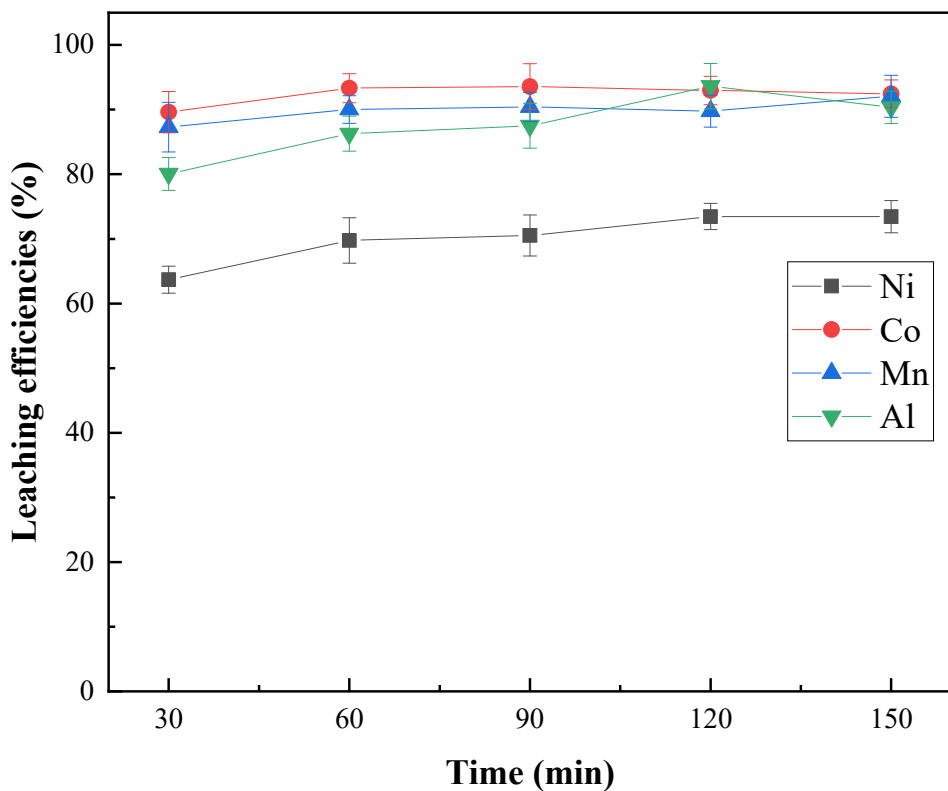


**Figure 9.** Effect of roasting time on leaching of each element ( $D_p/D_t = 1.2$ ,  $T = 180$  °C).

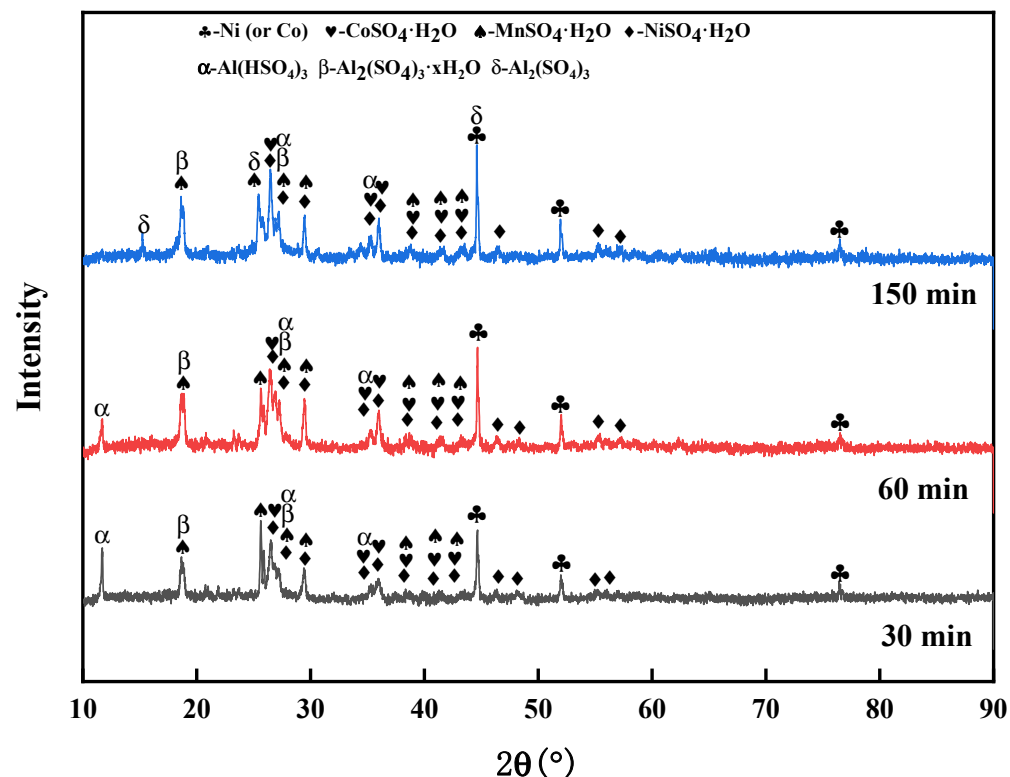


**Figure 10.** X-ray diffraction patterns of the roasted products after different roasting times in the sulfate roasting ( $D_p/D_t = 1.2$ ,  $T = 180\text{ }^\circ\text{C}$ ).

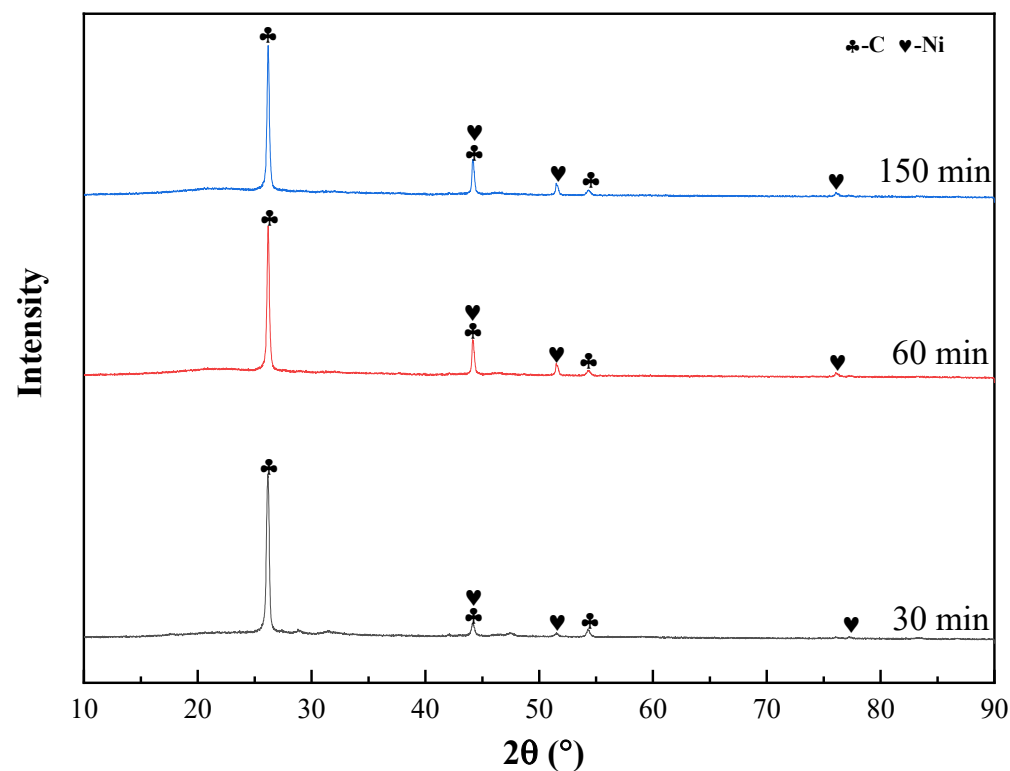


**Figure 11.** X-ray diffraction patterns of the water leaching residue after different roasting times ( $t = 120\text{ min}$ ,  $L/S = 10\text{ mL/g}$ ).

### 3.1.4. Effect of the Sulfuric Acid Amount

The effects of the sulfuric acid amount on the extractions of Ni, Co, Mn and Al are presented in Figure 12. The amount of sulfuric acid used had a significant effect on metal leaching. The efficiency for Ni extraction increased from 59.98% to 87.13% when the  $D_p/D_t$  (ratio of actual usage to theoretical usage of sulfuric acid) was increased from 1:1 to 1.4:1, and the extraction efficiencies for Co, Mn and Al increased substantially—Co: 82.92% to 99.87%; Mn: 83.06% to 96.20%; and Al: 84.63% to 94.94%, respectively. This is clearly illustrated in Figure 13, which shows that the main phases in the roasting product were  $\text{NiSO}_4 \cdot \text{H}_2\text{O}$ ,  $\text{CoSO}_4 \cdot \text{H}_2\text{O}$ ,  $\text{MnSO}_4 \cdot \text{H}_2\text{O}$  and  $\text{Al}_2(\text{SO}_4)_3 \cdot x\text{H}_2\text{O}$ . Sulfates are soluble in water and were introduced into the solution by water leaching, which explains the increased amounts of Ni, Co, Mn and Al extracted. When the sulfuric acid ratio was 1.1, Al existed mainly as  $\text{Al}_2(\text{SO}_4)_3 \cdot x\text{H}_2\text{O}$ , and when the sulfuric acid ratio was 1.2, Al existed as  $\text{Al}_2(\text{SO}_4)_3 \cdot \text{H}_2\text{O}$  and  $\text{Al}(\text{HSO}_4)_3$ . The increased sulfuric acid dosage contributed to the formation of  $\text{Al}(\text{HSO}_4)_3$ . Figure 14 shows that C, Ni and CoO were the main mineral phases after extraction with 1.1:1 sulfuric acid, which indicated that small amounts of Co and Ni failed to react completely when the sulfuric acid content was insufficient, and some of the Co reacted with oxygen in the air to form CoO. This explains the low extraction efficiencies for metal leaching. Further analyses of the leaching residue morphologies with SEM (Figure 15) verified that there were scaly crystals on the surface of the roasted product, and as the amount of sulfuric acid was increased, both scaly and fluffy crystals were found, and the number of crystals increased. This was consistent with the morphology of the sulfate.

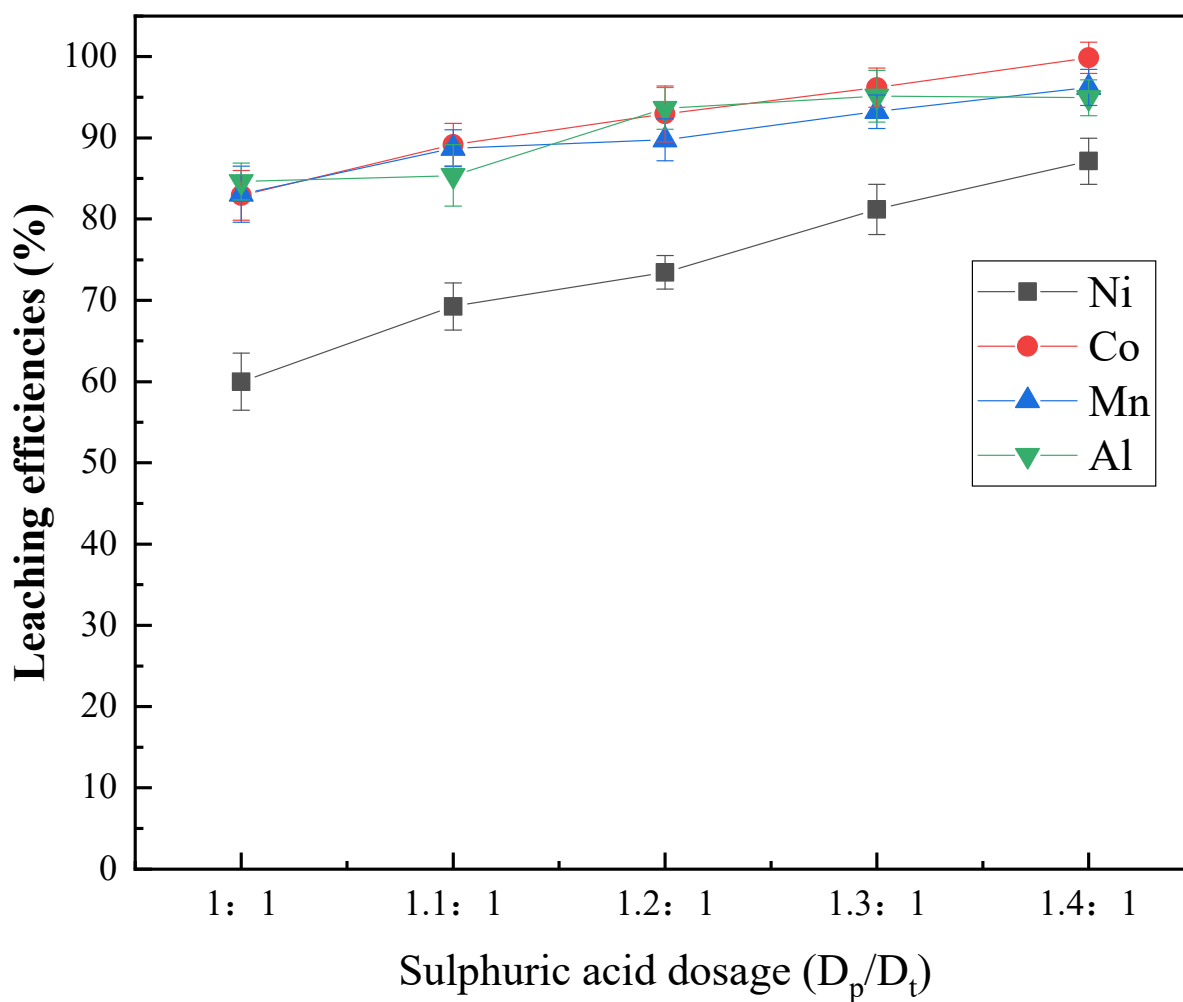


**Figure 12.** Effect of the sulfuric acid content on leaching of each element ( $T = 180\text{ }^\circ\text{C}$ ,  $t = 120\text{ min}$ ).

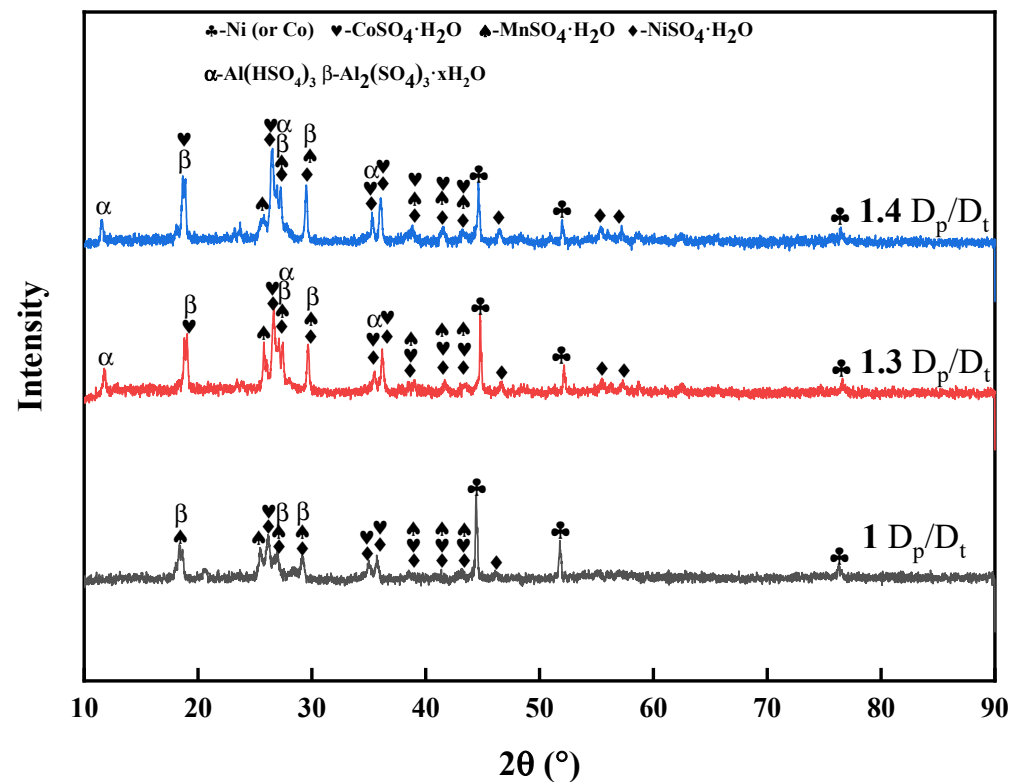


**Figure 13.** X-ray diffraction patterns for the roasted products with different sulfuric acid contents in the sulfate roasting ( $T = 180 \text{ }^{\circ}\text{C}$ ,  $t = 120 \text{ min}$ ).

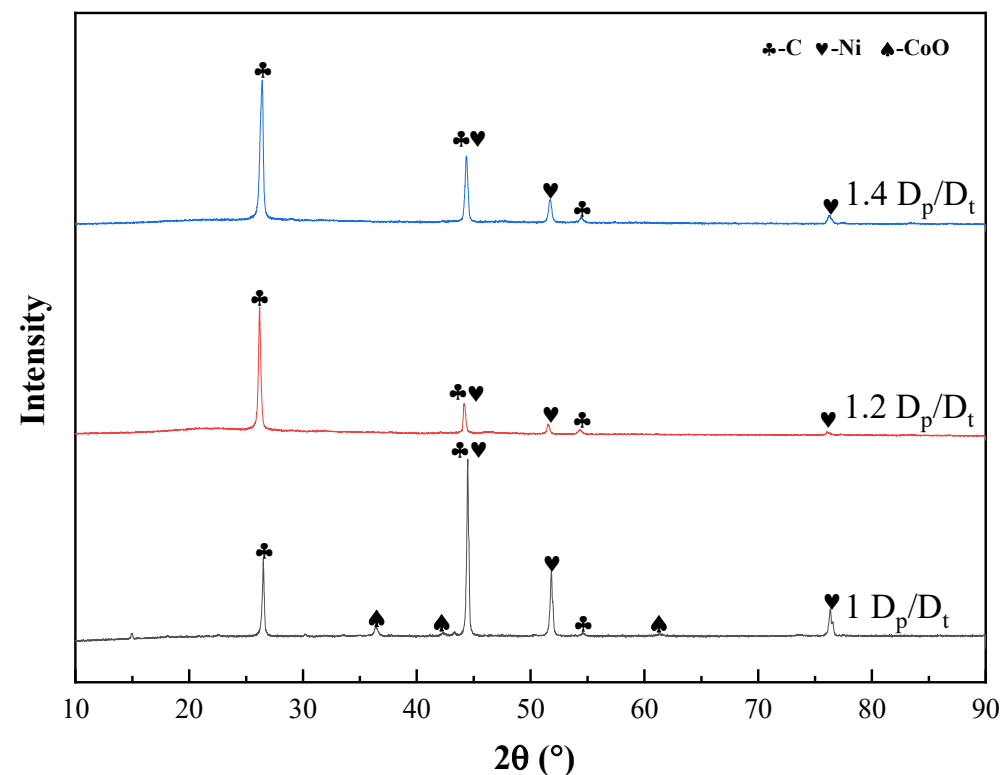


**Figure 14.** X-ray diffraction patterns for the water leaching residue obtained with different sulfuric acid amounts ( $t = 120 \text{ min}$ ,  $L/S = 10 \text{ mL/g}$ ).

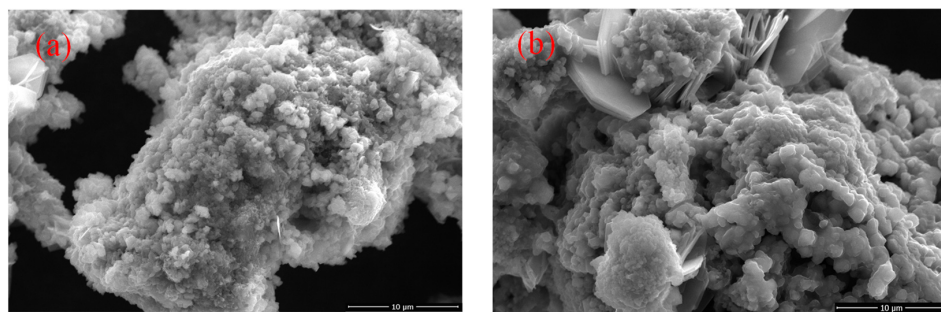


**Figure 15.** SEM images of the roasted product obtained with different sulfuric acid proportions: (a)  $D_p/D_t = 1.1$ ; (b)  $D_p/D_t = 1.4$ .

### 3.2. Selective Separation of Mn

The resultant solution was subjected to oxidative  $\text{MnO}_2$  precipitation with  $\text{KMnO}_4$ . The main reaction is shown in Equation (7).



$K_p$  was the actual amount of  $\text{KMnO}_4$ , and  $K_t$  was the theoretical amount of  $\text{KMnO}_4$ . The effect of the  $\text{KMnO}_4$  amount on the extraction of Co and Mn is presented in Figure 16a. The amount of Mn precipitated increased from 50.76% to 98.12% when the amount of  $\text{KMnO}_4$  was increased from 0.5 to 1.0, and the precipitation of Co remained nearly constant at 1%. When the amount of  $\text{KMnO}_4$  was increased from 1.0 to 1.5, the precipitation of Mn changed little, while the amount of Co precipitated increased to 4.00%. This is because the Co ions were oxidized to form a  $\text{Co}_3\text{O}_4$  precipitate [29]. Figure 17 and Table 3 present the SEM–EDS results for different spots, which confirm the presence of  $\text{MnO}_2$  as well as the main phases in the residues. Based on the above results, the optimal amount of  $\text{KMnO}_4$  was approximately 1.0.

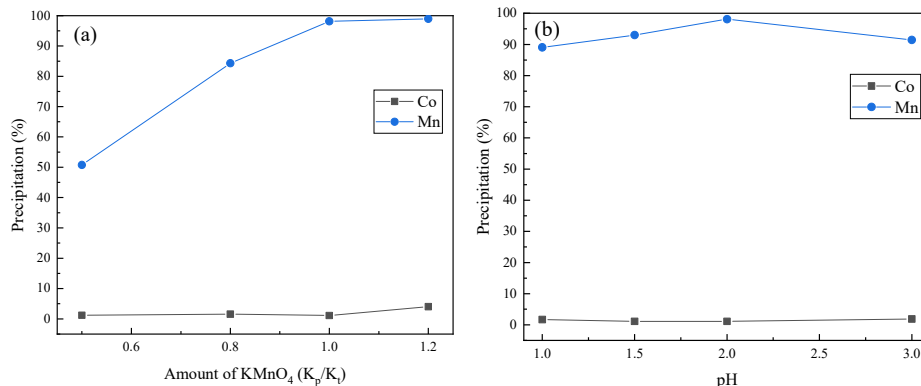


**Figure 16.** Effect of (a)  $\text{KMnO}_4$  dosage on the precipitation of Mn ( $T = 25^\circ\text{C}$ ;  $\text{pH} = 2$ ;  $t = 30\text{ min}$ ) and (b) pH on the precipitation of Mn ( $T = 25^\circ\text{C}$ ;  $K_p/K_t = 1$ ;  $t = 30\text{ min}$ ).

**Table 3.** SEM-EDS analysis results of the spots shown in Figure 17.

Spectrum	O	Mn	Co	Ni	Al	K	Fe	Cu	S
1	65.53	30.80	1.89	0.00	0.20	0.19	0.55	0.60	0.25
2	72.54	24.34	1.51	0.02	0.42	0.26	0.60	0.13	0.18
3	72.43	24.87	1.34	0.00	0.22	0.16	0.50	0.23	0.25
4	71.11	26.05	1.22	0.01	0.20	0.28	0.37	0.50	0.25
5	70.05	26.78	0.94	0.35	0.37	0.15	0.32	0.82	0.22

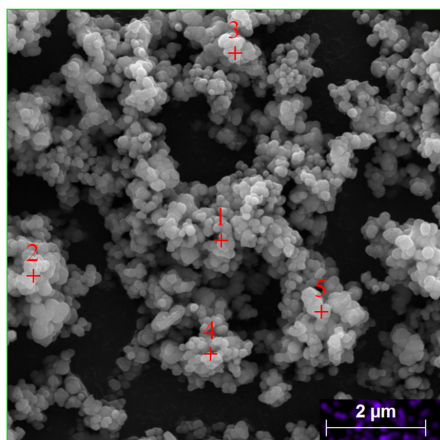


**Figure 17.** SEM-EDS image of the  $\text{MnO}_2$  product.

The effect of pH on the extraction of Co and Mn is presented in Figure 16b. The efficiency of Mn precipitation increased from 85.06% to 98.12% when the pH was increased from 1.0 to 2.0, and the rate of Co precipitation remained nearly constant at 1%. When the pH was increased from 2.0 to 3.0, the efficiency for Mn precipitation decreased from 94.00% to 87.43%, and the amount of Co remained nearly constant at 1%. This was ascribed to incomplete oxidation of Mn(II) to Mn(IV) and generation of the intermediate manganese product  $\text{MnO(OH)}$  [30]. Based on the above results, the optimal pH was approximately 2.0.

### 3.3. Removal of Al from the Water Leaching Solution

The effect of saponification rate on Al leaching is presented in Figure 18a. The extraction efficiency for Al initially increased substantially from 29.85% to 98.17% as the saponification rate was increased from 0% to 60%. Based on these results, the optimal saponification rate for the extraction of Al was approximately 60%. This is because the extractant P204 is an acidic extractant, and the extraction mechanism involves  $\text{Al}^{3+}$  extraction into the organic phase after reacting with the P-O-H in P204, and as the extraction proceeds, the displaced  $\text{H}^+$  reduces the pH of the solution to impede the diffusion of metal ions into the organic phase. The use of NaOH for saponification of the organic phase allowed  $\text{H}^+$  exchange with  $\text{Na}^+$  to ensure the extraction power of the targeted ions. Saponification removed the hydrophilic groups of the phosphoric acid that repelled metal ions, increasing the unsaturation and complexation ability of P204. This ability enhanced the interactions between P204 and the metal ions, thereby increasing the partition coefficients and extraction efficiencies. Furthermore, the saponification reaction increased the pH of the aqueous phase by using a strong base such as NaOH. This led to an increase in the solubility of the metal, slowed hydrolysis of the metal ions and accelerated the formation of complexes, ultimately resulting in increased extraction rates.

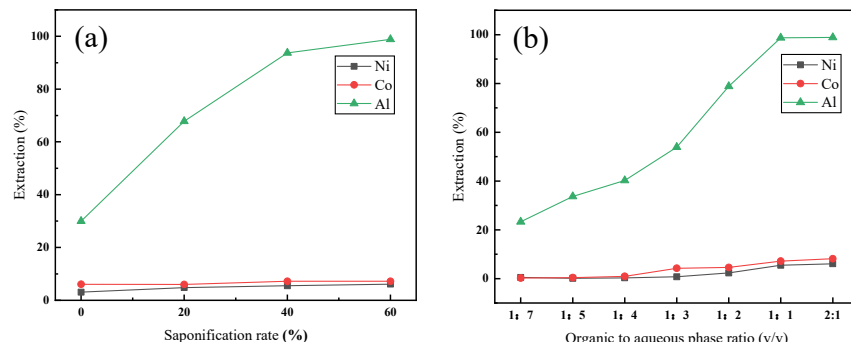


**Figure 18.** Effect of (a) saponification rate on the extraction of Al ( $\text{O}/\text{A} = 1:1$ ;  $T = 25^\circ\text{C}$ ;  $t = 30$  min;  $\text{pH} = 3.5$ ; P204 = 20% ( $v/v$ )); and (b) organic-to-aqueous phase ratio of Al (saponification rate = 60%;  $T = 25^\circ\text{C}$ ;  $t = 30$  min;  $\text{pH} = 3.5$ ; P204 = 20% ( $v/v$ )); TBP = 10% ( $v/v$ )).

The effect of the organic/aqueous phase ratio on Al leaching is presented in Figure 18b. The efficiency of Al extraction initially increased substantially from 23.29% to 98.73% and from 0.47% and 0.24% to 5.49% and 7.18% for Ni and Co, respectively, as the organic/aqueous phase ratio was increased from 1:7 to 1:1, indicating that most of the Al was extracted into the organic phase and enabled better separation of Ni, Co and Mn. With increases in the organic/aqueous phase ratio, the extraction efficiencies for Al, Ni, Co and Mn showed little change. Based on the above results, the optimal organic-to-aqueous phase ratio for Al removal was approximately 1:1.

### 3.4. Flowsheet Development

Based on these results, a new process for the recovery of Ni, Co, Mn, Al and Cu from priority lithium extraction residue based on sulfation roasting, water leaching and solvent extraction is outlined in Figure 19. The application of this new process could significantly improve the separation and recovery of Ni, Co, Mn, Al and Cu from priority lithium extraction residue. Mn was selectively separated and precipitated with  $\text{KMnO}_4$ . Then, the problem of difficult impurity removal from Al was resolved with a solvent extraction method. After extraction and separation, a solution containing aluminum was obtained, and aluminum hydroxide or alumina powder could be prepared through the hydrolysis precipitation process. Finally, nickel sulfate and cobalt sulfate products were further prepared from Al-free solution through stepwise solvent extraction. This reduced the environmental impacts of this novel approach and optimized the production process.

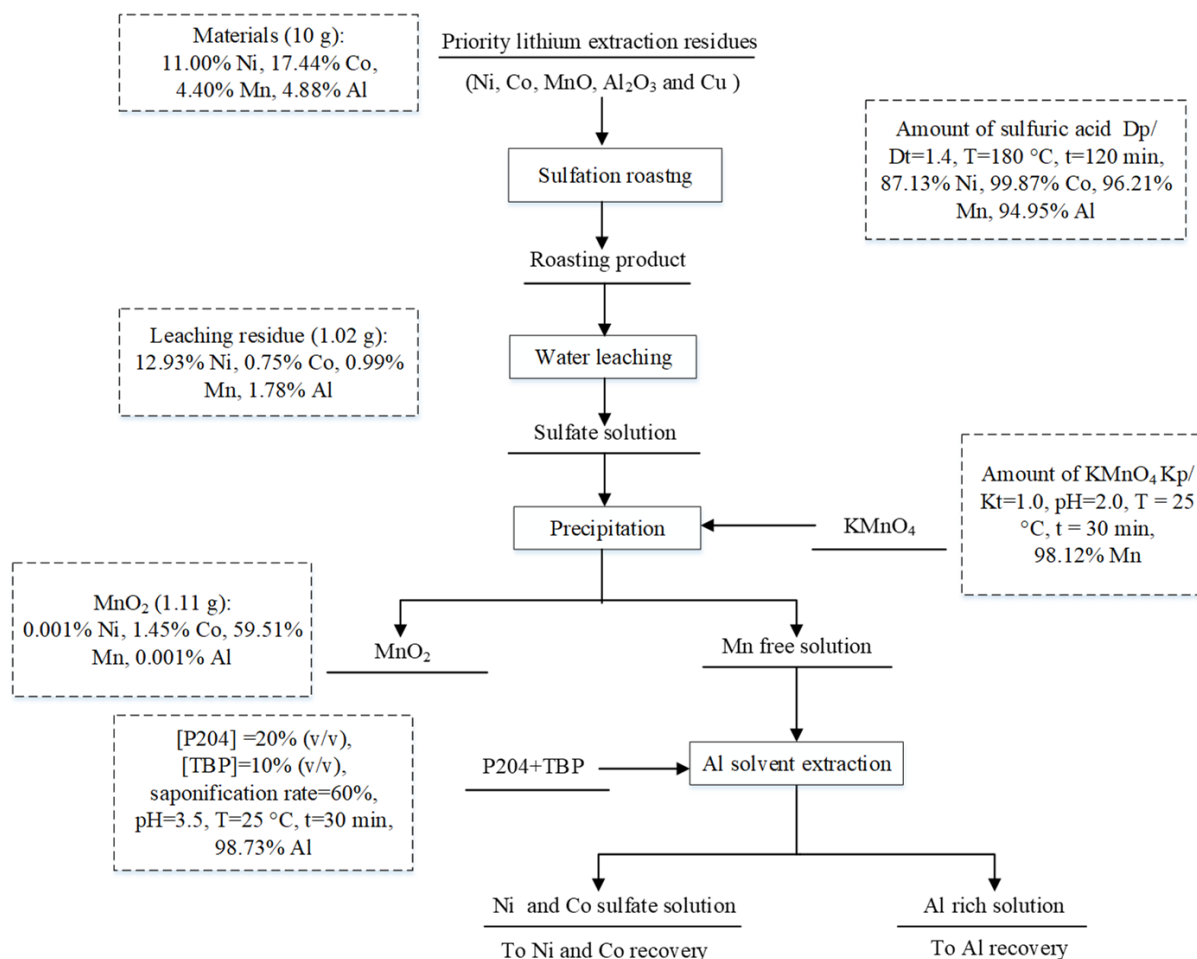


**Figure 19.** Proposed flow sheet for recovery of Ni, Co, Mn and Al from priority lithium extraction residues.

#### 4. Conclusions

- (1) A sulfation roasting–water leaching process enabled the efficient extraction of Ni, Co and Mn from priority lithium residues obtained from the hydrogen reduction of spent lithium ternary batteries. More than 87% Ni, 99% Co and 96% Mn were extracted at 180 °C and 120 min with 1.4 times the theoretical amount of sulfuric acid.
- (2) More than 98% of the Mn was selectively separated and precipitated under the optimal conditions. Al was also separated through extraction with P2O5 from the leaching solution. More than 98% of the Al was extracted with 20% (v/v) P2O5 + 10% (v/v) TBP at an A/O ratio of 1:1 within 30 min at 30 °C.
- (3) This optimized and efficient process for the extraction of valuable metals from priority extraction lithium residues increased the feasibility of hydrogen reduction treatment for waste lithium batteries and enabled industrialization of the new process. The proposed new process not only achieves efficient recovery of valuable metals such as lithium, nickel, cobalt, manganese, etc., but also has advantages such as high efficiency, low energy consumption and environmental protection.

**Author Contributions:** Literature search, Y.G. and F.L.; study design, Y.G. and F.L.; investigation, H.Z. and T.Z.; data collection, Y.G. and C.S.; data analysis, Y.G. and F.C.; data interpretation, Y.G.; writing, Y.G. and F.L.; review and editing, F.L. and Z.C. All authors have read and agreed to the published version of the manuscript.

**Funding:** This paper was financially supported by the Training Plan for Academic and Technical Leaders of Major Disciplines in Jiangxi Province (20225BCJ23009), the Major Science and Technology Research Projects in Yichun City (2023ZDKJGG01), the Unveiling and commanding project in Jiangxi Province (20213AAE02010), the Postdoctoral Innovative Talent Support Program of Shandong Province and Program of Qingjiang Excellent Young Talents, Jiangxi University of Science and Technology (No. JXUSTQJYX2019006), the Jiangxi Postdoctoral Science Foundation (No. 2019 KY07), the Natural Science Foundation for Distinguished Young Scholars of Jiangxi Province (No.20232ACB214006), and Jiangxi Provincial Key Laboratory of Flash Green Development and Recycling (No. 20193BCD40019).

**Data Availability Statement:** The data presented in this study are available upon request from the corresponding author. The data are not publicly available due to privacy.

**Conflicts of Interest:** The authors declare no conflicts of interest. The funders had no role in the design of the study; in the collection, investigation, analyses, or interpretation of the data; in the writing of the manuscript; or in the decision to publish the results.

#### References

1. Gastol, M.; Marshall, J.; Cooper, E.; Mitchell, C.; Burnett, D.; Song, T.; Sommerville, R.; Middleton, B.; Crozier, M.; Smith, R.; et al. Reclaimed and Up-Cycled Cathodes for Lithium-Ion Batteries. *Glob. Chall.* **2022**, *6*, 2200046. [[CrossRef](#)] [[PubMed](#)]
2. Xiong, S.Q.; Ji, J.P.; Ma, X.M. Environmental and economic evaluation of remanufacturing lithium-ion batteries from electric vehicles. *Waste Manag.* **2020**, *102*, 579–586. [[CrossRef](#)] [[PubMed](#)]
3. Gruber, P.W.; Medina, P.A.; Keoleian, G.A.; Kesler, S.E.; Everson, M.P.; Wallington, T.J. Global Lithium Availability A Constraint for Electric Vehicles? *J. Ind. Ecol.* **2011**, *15*, 760–775. [[CrossRef](#)]
4. Li, F.H.; Yang, J.Y. Research progress on recovery of cathode materials from spent lithium batteries. *Mod. Chem. Ind.* **2021**, *41*, 90–94.
5. Sonoc, A.; Jeswiet, J. A Review of Lithium Supply and Demand and a Preliminary Investigation of a Room Temperature Method to Recycle Lithium Ion Batteries to Recover Lithium and Other Materials. *Procedia CIRP* **2014**, *15*, 289–293. [[CrossRef](#)]
6. Swain, B. Recovery and recycling of lithium: A review. *Sep. Purif. Technol.* **2017**, *172*, 388–403. [[CrossRef](#)]
7. Sonoc, A.; Jeswiet, J.; Soo, V.K. Opportunities to Improve Recycling of Automotive Lithium Ion Batteries. *Procedia CIRP* **2015**, *29*, 752–757. [[CrossRef](#)]
8. Du, G.C.; Zheng, L.L.; Zhang, Z.C.; Feng, Y.; Wang, D.; Dai, Z.Q. Overview of research on thermal safety of lithium-ion batteries. *Energy Storage Sci. Technol.* **2019**, *8*, 500–505.
9. Li, J.G.; Zhao, R.S.; He, X.M.; Liu, H.C. Preparation of LiCoO<sub>2</sub> cathode materials from spent lithium-ion batteries. *Ionics* **2009**, *15*, 111–113. [[CrossRef](#)]
10. Yang, J.; Qin, J.; Li, F.C.; Jiang, L.X.; Lai, Y.Q.; Liu, F.Y.; Jia, M. Review of hydrometallurgical processes for recycling spent lithium-ion batteries. *J. Cent. South Univ. (Sci. Technol.).* **2020**, *51*, 3261–3278.

11. Liu, G.Q.; Wang, F. Status of Power Lithium Ion Battery Recycle Technology. *China Resour. Compr. Util.* **2018**, *36*, 88–92.
12. Wang, F.; Zhang, B.S.; Liu, G.Q.; Xie, X. Progress in Recycling Technology of Waste Power Battery Resources. *China Resour. Compr. Util.* **2018**, *36*, 106–111.
13. Ren, G.; Xiao, S.; Xie, M.; Pan, B.; Fan, Y.; Wang, F.; Xia, X. Recovery of Valuable Metals from Spent Lithium-Ion Batteries by Smelting Reduction Process Based on MnO-SiO<sub>2</sub>-Al<sub>2</sub>O<sub>3</sub> Slag System. In *Advances in Molten Slags, Fluxes, and Salts: Proceedings of the 10th International Conference on Molten Slags, Fluxes and Salts 2016, Washington, DC, USA, 22–25 May 2016*; Springer: Berlin/Heidelberg, Germany, 2016; pp. 211–218.
14. Heydarian, A.; Mousavi, S.M.; Vakilchap, F.; Baniasadi, M. Application of a mixed culture of adapted acidophilic bacteria in two-step bioleaching of spent lithium-ion laptop batteries. *J. Power Sources* **2018**, *378*, 19–30. [[CrossRef](#)]
15. Yao, Y.L.; Zhu, M.Y.; Zhao, Z.; Tong, B.H.; Fan, Y.Q.; Hua, Z.S. Hydrometallurgical Processes for Recycling Spent Lithium-Ion Batteries: A Critical Review. *ACS Sustain. Chem. Eng.* **2018**, *6*, 13611–13627. [[CrossRef](#)]
16. Gu, F.; Guo, J.F.; Yao, X.; Summers, P.A.; Widijatmoko, S.D.; Hall, P. An investigation of the current status of recycling spent lithium-ion batteries from consumer electronics in China. *J. Clean. Prod.* **2017**, *161*, 765–780. [[CrossRef](#)]
17. Tong, Z.; Ren, X.B.; Ni, M.Q.; Bu, X.N.; Dong, L.S. Review of Ultrasound-Assisted Recycling and Utilization of Cathode Materials from Spent Lithium-Ion Batteries: State-of-the-Art and Outlook. *Energy Fuels* **2023**, *37*, 14574–14588. [[CrossRef](#)]
18. Wang, D.; Zhang, X.; Chen, H. Separation of Li and Co from the active mass of spent Li-ion batteries by selective sulfat-ing roasting with sodium bisulfate and water leaching. *Miner. Eng.* **2018**, *126*, 28–35. [[CrossRef](#)]
19. Peng, C.; Liu, F.; Wang, Z. Selective extraction of lithium (Li) and preparation of battery grade lithium carbonate (Li<sub>2</sub>CO<sub>3</sub>) from spent Li-ion batteries in nitrate system. *J. Power Sources* **2019**, *415*, 179–188. [[CrossRef](#)]
20. Zhang, J.L.; Hu, J.T.; Zhang, W.J. Efficient and economical recovery of lithium, cobalt, nickel, manganese from cathode scrap of spent lithium-ion batteries. *J. Clean. Prod.* **2018**, *204*, 437–446. [[CrossRef](#)]
21. Hu, J.; Zhang, J.; Li, H. A promising approach for the recovery of high value-added metals from spent lithium-ion batteries. *J. Power Sources* **2017**, *351*, 192–199. [[CrossRef](#)]
22. Xu, P.; Zhang, X.H.; Ma, E. Selective Recovery of Lithium from Spent Lithium-ion Batteries Synergized by Carbon and Sulfur Elements. *Acta Chim. Sin.* **2021**, *79*, 1073–1081. [[CrossRef](#)]
23. Xu, P.; Liu, C.W.; Zhang, X.H. Synergic Mechanisms on Carbon and Sulfur during the Selective Recovery of Valuable Metals from Spent Lithium-Ion Batteries. *ACS Sustain. Chem. Eng.* **2021**, *9*, 2271–2279. [[CrossRef](#)]
24. Liu, F.; Peng, C.; Ma, Q.; Wang, J.; Zhou, S.; Chen, Z.; Wilson, B.P.; Lundström, M. Selective lithium recovery and integrated preparation of high-purity lithium hydroxide products from spent lithium-ion batteries. *Sep. Purif. Technol.* **2021**, *259*, 118181. [[CrossRef](#)]
25. Zheng, H.S.; Dong, T.; Sha, Y.F.; Jiang, D.F.; Zhang, H.T.; Zhang, S.J. Selective Extraction of Lithium from Spent Lithium Batteries by Functional Ionic Liquid. *ACS Sustain. Chem. Eng.* **2021**, *9*, 7022–7029. [[CrossRef](#)]
26. Sun, L.; Qiu, K.Q. Vacuum pyrolysis and hydrometallurgical process for the recovery of valuable metals from spent lithium-ion batteries. *J. Hazard. Mater.* **2011**, *194*, 378–384. [[CrossRef](#)] [[PubMed](#)]
27. Huang, B.; Pan, Z.F.; Su, X.Y.; An, L. Recycling of lithium-ion batteries: Recent advances and perspectives. *J. Power Sources* **2018**, *399*, 274–286. [[CrossRef](#)]
28. Bale, C.W.; Bélisle, E.; Chartrand, P.; Dechterov, S.A.; Eriksson, G.; Gheribi, A.E.; Hack, K.; Jung, I.-H.; Kang, Y.-B.; Melançon, J.; et al. FactSage thermochemical software and databases, 2010–2016. *Calphad Comput. Coupling Phase Diagr. Thermochem.* **2016**, *54*, 35–53. [[CrossRef](#)]
29. Peng, C.; Chang, C.; Wang, Z.; Wilson, B.P.; Liu, F.; Lundström, M. Correction to: Recovery of High-Purity MnO<sub>2</sub> from the Acid Leaching Solution of Spent Li-Ion Batteries. *JOM J. Miner. Met. Mater. Soc.* **2020**, *72*, 978. [[CrossRef](#)]
30. Huang, Y.; Han, G.; Liu, J.; Chai, W.; Wang, W.; Yang, S.; Su, S. A stepwise recovery of metals from hybrid cathodes of spent Li-ion batteries with leaching-flotation-precipitation process. *J. Power Sources* **2016**, *325*, 555–564. [[CrossRef](#)]

**Disclaimer/Publisher’s Note:** The statements, opinions and data contained in all publications are solely those of the individual author(s) and contributor(s) and not of MDPI and/or the editor(s). MDPI and/or the editor(s) disclaim responsibility for any injury to people or property resulting from any ideas, methods, instructions or products referred to in the content.